Journal of Alloys and Compounds 654 (2016) 514–522

Contents lists available at ScienceDirect

Journal of Alloys and Compounds

journal homepage: http://www.elsevier.com/locate/jalcom

Electrochemical synthesis of TiO_2/Graphene oxide composite films for photocatalytic applications

Anderson Guimarães de Oliveira [a], Jefferson Patrício Nascimento [b], Honória de Fátima Gorgulho [a, *], Patrícia Benedini Martelli [a], Clascídia Aparecida Furtado [b], José Luís Figueiredo [c]

[a] (UFSJ) Universidade Federal de São João del Rei, Praça Dom Helvécio 74, CEP36300-000, São João del Rei, Minas Gerais, Brazil
[b] (CDTN) Laboratório de Química de Nanoestruturas, Centro de Desenvolvimento da Tecnologia Nuclear, Belo Horizonte, Minas Gerais, Brazil
[c] Laboratório Associado LSRE-LCM, Departamento de Engenharia Química, Faculdade de Engenharia, Universidade do Porto, Rua Dr. Roberto Frias, 4200-465, Porto, Portugal

ARTICLE INFO

Article history:
Received 15 May 2015
Received in revised form
4 September 2015
Accepted 13 September 2015
Available online 14 September 2015

Keywords:
Graphene
TiO_2-Graphene composite
Photocatalytic degradation
Electrochemical deposition

ABSTRACT

This paper presents a novel TiO_2-Graphene composite film one-step preparation method by electrochemical synthesis. The films were prepared on a Ti substrate by electrochemical deposition from a GO and Ti (IV) aqueous solution. For comparison, pure TiO_2 on a Ti substrate was obtained by the same electrochemical method. The as-prepared samples were characterized by X-ray diffraction, scanning electron microscopy, Raman spectroscopy, photoluminescence and ultraviolet–visible spectrophotometry. The photocatalytic properties of the films were investigated for the discoloration of Reactive Yellow 145 dye. The results showed that the TiO_2-Graphene oxide composite film presented photocatalytic activity almost twice as high as that observed for the TiO_2 film. In addition, the TiO_2-Graphene oxide composite film presented better stability and recyclability, retaining its catalytic efficiency ($\approx$70%) even after 15 cycles.

Published by Elsevier B.V.

1. Introduction

TiO_2 is one of the most important materials in the field of photocatalytic waste water purification [1–3]. In addition to its outstanding photocatalytic properties, TiO_2 presents good stability, is not toxic and has a low cost, making it one of the main components of the new materials developed for the photocatalytic treatment of waste water. The major limitation concerning its applicability is its narrow sun light range absorbance, which results in a very low efficiency [3–5]. When TiO_2 is irradiated by light with energy higher than its bandgap, an electron–hole pair is generated at the surface. The photon-induced electrons and holes have a strong oxidizing power, but their oxidation ability is limited by their fast recombination rates, leading to a low photocatalytic activity. In order to overcome these problems, several strategies have been employed. One of the most promising approaches to tackle this limitation is the combination of TiO_2 with carbon nanomaterials, such as carbon nanotubes [6–8], fullerene C60 [8], graphene-based materials [8–11], and nanodiamonds [12].

Previous studies have demonstrated that combining TiO_2 with graphene oxide (GO) or reduced graphene oxide (rGO) can decrease the electron–hole recombination rate, thus lowering its gap energy and enhancing its photocatalytic performance [8,9,13,14]. However, many studies have shown that the photocatalytic activity of these composites is significantly affected by the material textural and morphological properties [9–12]. The preparation of GO/TiO_2 and rGO/TiO_2 composites usually involves complex experimental procedures, because of the poor interfacial contact of the oxide particles with the carbon surface and their tendency to agglomerate. Some studies claim that increasing the proportion of carbon in these composites may improve their photocatalytic activity by favoring the adsorption of the pollutant [15,16].

However, recent studies have shown that there is an optimum GO-TiO_2 ratio for maximum photocatalytic activity [8,9]. The carbon material concentration may affect the interaction between TiO_2 and rGO or GO particles, which is the main feature required to enhance charge separation and electron transfer. J. Yang et al.

* Corresponding author. Permanent address: Universidade Federal de São João del Rei, Praça Dom Helvécio 74, CEP 36301-160, São João del Rei, Minas Gerais, Brazil.
E-mail address: gorgulho@ufsj.edu.br (H. de Fátima Gorgulho).

http://dx.doi.org/10.1016/j.jallcom.2015.09.110
0925-8388/Published by Elsevier B.V.

investigated TiO_2-Graphene microspheres prepared by ultrasonic spray pyrolysis and suggested that a higher graphene content may limit the contact of the TiO_2 surface with the pollutant and reduce the photocatalytic activity [16]. W. Jo et al. also investigated the photocatalytic activity of a GO/TiO_2 composite synthesized by a colloidal blending process [17] and also observed that a higher GO content in the composites decreased the degradation efficiency. More recently, the oxygen functionalities in GO have been found to be essential to mediate a uniform assembly of TiO_2 nanoparticles onto GO sheets with ensuing improved photocatalytic performance in comparison to rGO-based composites [11].

The present work reports a new single-step method to obtain TiO_2/GO composites by electrochemical synthesis. A Ti plate was used as a substrate for TiO_2/GO composite film preparation by electrochemical deposition from a GO-Ti(IV) aqueous solution. Ti(IV) was added to the solution using K_2TiF_6, which is soluble in water and therefore will produce the hydrolysis of Ti(IV) species. This strategy exploits the simultaneous deposition of TiO_2 and GO onto the substrate by cyclic voltammetry (CV). For comparison, pure TiO_2 on Ti substrate was obtained by the same electrochemical method, but without GO added to the electrolyte solution. The prepared TiO_2/GO composite and TiO_2 films were tested in the photocatalytic decolorization of Reactive Yellow 145, a dye used in the textile industry.

2. Experimental section

2.1. Graphene oxide preparation and purification

GO was prepared through oxidation of natural nanographite (99.5 wt% of purity), supplied by the *Brazilian Company Nacional de Grafite Ltda*. The oxidation procedure used H_2SO_4, KMnO4 and H_2O_2, based on Hummers method [18]. The oxidation product was first washed with HCl (10%), then filtered and dried at 65 °C, and finally purified by subsequent washing with aqueous NaOH/water at pH 7, ethanol, and ether to remove oxidized carbonaceous residues. Finally, GO was filtered on a PTFE membrane with a pore diameter of 0.45 μm and dried for 24 h at 100 °C under vacuum [19].

2.2. Ti/TiO_2 and TiO_2/GO composite film preparation

A 2-mm thick pure Ti plate with a geometric area of 30 cm^2 was employed as a working electrode onto which the TiO_2 and graphene oxide (GO) film were electrochemically deposited. The Ti-plate surface was sequentially ground with a 360–2000-grit SiC paper, rinsed with acetone, ultrasonically cleaned in isopropyl alcohol for 20 min, and then preserved in isopropyl alcohol until further use. A platinum wire connected to the Ti-plate provided electrical contact to the working electrode. A three-electrode cell (200 mL) was used in all experiments. Platinum foil (30 cm^2) was used as a counter electrode and an Ag/AgCl electrode was used as a reference. The CV experiments were performed using Autolab Electrochemical System (EcoChemie, Utrecht, The Netherlands) equipped with PGSTAT-12 and GPES software. In order to obtain the TiO_2/GO film, the electrochemical experiments were conducted using a mixture of 15 mg of GO and 100 mg of K_2TiF_6 in 150 mL of phosphate buffer at pH 9.0 as a support electrolyte. The sample obtained was labeled Ti/TiO_2/GO. The Ti/Ti/TiO_2 film was prepared using 100 mg of K_2TiF_6 in 150 mL phosphate buffer at pH 9.0 as a support electrolyte. The CV experiments were carried out over the potential range from −1.0–5.0 V at a scan rate of 50 mV s^{-1}. For comparison, a Ti/TiO_2 sample was prepared using only the phosphate buffer at pH 9.0 as a support electrolyte. Table 1 summarizes the preparation conditions of the prepared samples.

2.3. Characterization

Fourier-transform Raman spectroscopy was conducted using a Bruker RFS 100 instrument, a Nd^{3+}/YAG laser operating in near-infrared at 1064 nm and a liquid N_2-cooled charge-coupled device detector. Good signal-to-noise ratios were obtained with 1000 scans accumulated over approximately 30 min and 4-cm^{-1} spectral resolution. Surface morphology observations were obtained by scanning electron microscopy (SEM) with a Quanta 200 - FEG - FEI − 2006 unit. The samples were attached to a metal sample holder with adhesive carbon tape. X-Ray diffraction of the Ti-plate samples was performed by using a Shimadzu XRD-6000 diffractometer operating with $\lambda = 0.15418$ nm at 30 kV and 30 mA and a step size of 0.02°. Diffuse Reflectance Ultraviolet–Visible Spectroscopy (DRUV) was conducted on a Cary 5000-UV–Vis-NIR Spectrophotometer (Agilent Technologies) using an external diffuse reflectance accessory. Photoluminescence (PL) spectra were measured on a RF-5301PC Spectrofluorophotometer (Shimadzu). The samples were excited at the wavelength of 350 nm with a 150-W Xenon lamp under ambient conditions.

2.4. Photocatalytic tests

The photocatalytic performance of Ti/Ti/TiO_2 and Ti/TiO_2/GO composite films were evaluated in the discoloration of Reactive Yellow 145 using two 15-W ultraviolet–visible (UV–Vis) light lamps with spectral output from 250 to 1000 nm, and peak activity between 400 and 800 nm. A 150-mL reaction flask with a cooling jacket was placed 30 cm away from the light sources. The Ti substrate containing the composite film was placed into the reaction flask and one side (area of 30 cm^2) was exposed to the light sources. All the experiments were performed using 70 mL of a synthetic aqueous solution of 10 mgL^{-1} of Reactive Yellow 145 and textile dyeing bath samples containing around 8.5 mgL^{-1} of the such dye. Before starting the photocatalytic reaction, the solution was stirred for 30 min in the dark to achieve adsorption equilibrium. After that, the light was switched on in order to start the photocatalytic reaction. The dye concentration was determined measuring the amount of light absorbed at 420 nm by means of a Cary-50 UV–Vis spectrophotometer. The photo-discoloration rate was evaluated by measuring the dye concentration as function of time in the first 10 min.

3. Results and discussion

Surface modification of the Ti substrate was detected through changes in the CV profile, displayed in Fig. 1(a–c). The similarity between the substrate CVs indicates the formation of TiO_2, which probably is the major electrochemical process that occurred in the electrode. Indeed, as soon as CV was performed between potentials −1.0 and +5.0 V, TiO_2 formation was demonstrated by the anodic current peaks centered at 0.89 V and 2.15 V [20,21]. Thus, the oxide layer began to form during anodic oxidation, inhibiting further Ti dissolution. Hence, after the first scan, the current decreased significantly due to electrode surface passivation by the oxide layer, which increased the Ti surface charge transfer resistance.

The effect of the addition of the Ti(IV) salt to the electrolyte can be observed in the CV of sample Ti/Ti/TiO_2 showed in Fig. 1(b). In this case, the anodic peak was observed mainly at a higher potential (2.67 V). The oxidation potential increase is reported in the literature as resulting from different oxide growth rates on different single grains on the titanium substrate, and also from the oxide phase transformation [22,23]. Indeed, although TiO_2 is more stable and frequently found in the oxide film, different Ti oxides can be

Table 1
Support electrolytes employed in the electrochemical preparation of each sample.

Sample	Support electrolyte
$Ti/Ti/TiO_2$	K_2TiF_6 solubilized in phosphate buffer at pH 9.0
$Ti/TiO_2/GO$	GO dispersion and K_2TiF_6 solubilized in phosphate buffer at pH 9.0
Ti/TiO_2	Phosphate buffer at pH 9.0

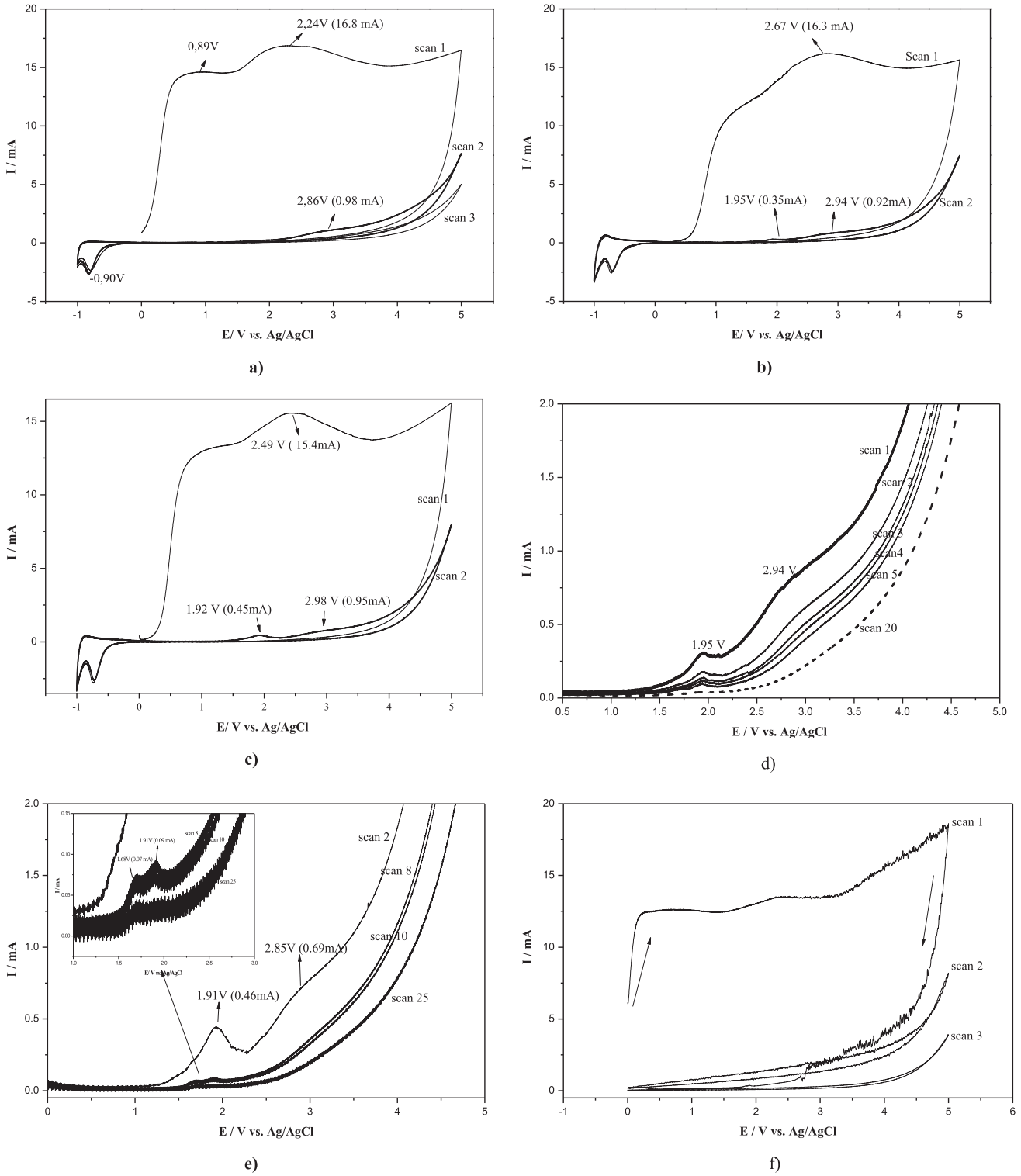

Fig. 1. Cyclic voltammograms recorded at 50 mV^{-1} for TiO_2 growth in phosphate buffer solution at pH 9.0: a) Ti/TiO_2; b) $Ti/Ti/TiO_2$ and c) $Ti/TiO_2/GO$; d) Anodic CV peaks observed during the positive scan for $Ti/Ti/TiO_2$; e) Anodic CV peaks observed during the positive scan for $Ti/TiO_2/GO$ and Inset: anodic curves for scans 8, 10 and 25 for $Ti/TiO_2/GO$ and f) Cyclic voltammograms with cathodic sweep limited to 0 V for $Ti/Ti/TiO_2$.

formed on the Ti surface during anodic oxidation, such as Ti_4O_7, Ti_3O_5 and Ti_2O_3. A similar behavior was observed in the CV for Ti/TiO_2/GO, shown in Fig. 1(c), which has a main anodic peak at 2.49 V. The Ti/Ti/TiO_2 and Ti/TiO_2/GO second scans showed two anodic peaks, one around 1.90 V and another poorly defined around 2.90 V. These peaks can be better observed in Fig. 1(d) and 1e. It can be noticed that the last anodic peak practically vanished in the other scans, while the first peak gradually decreased, but did not vanish with the number of scans. The presence of these anodic peaks even after several CV cycles suggests that several layers of oxides were formed in the process. Thus, the addition of K_2TiF_6 to the electrolyte produced hydrolyzed Ti(IV), contributing to the formation of an oxide layer denser than that observed for Ti/TiO_2.

The cathodic current peak observed at −0.73 V is attributed to the partial reduction of more superficial oxides and the peak at −1.00 V is attributed to the reduction of H^+. This assignment is supported by the result shown in Fig. 1(f) for sample Ti/Ti/TiO_2, where by limiting the cathodic sweep to 0 V, the anodic peaks observed around 2.0 V and 3.0 V vanished.

In the case of Ti/TiO_2/GO, after the first scan, the anodic peak split into two other peaks, located at 1.68 V (0.07 mA) and 1.89 V (0.09 mA), as shown in inset in Fig. 1(d). It seems that two different deposition processes took place on the electrode surface with the probable formation of two layers. The peak at a more positive potential (1.89 V) possibly originated from the TiO_2/GO film accumulated in a layer deeper than that at a less positive potential (1.68).

The surfaces of the as-prepared films on the Ti substrate were analyzed by X-ray diffraction; the results are shown in Fig. 2. The XRD patterns attributed to the Ti substrate occurred at about $2\theta = 35.2°$, 38.5°, 40.4°, 53.1°, 63.1°, 76.2° and 77.5° corresponding to diffractions from the (100), (002), (101), (102), (110), (112) and (201) planes, respectively [24,25]. After CV cycling between potentials −1.0 V and +5.0 V, Ti/TiO_2 still presented peaks attributed to pure Ti. The absence of typical TiO_2 peaks may be related to low TiO_2 crystallization during the anodizing process. Additionally, the smaller thickness of the oxide film may lead to thin-film interference problems [25]. However, the XRD patterns for Ti/Ti/

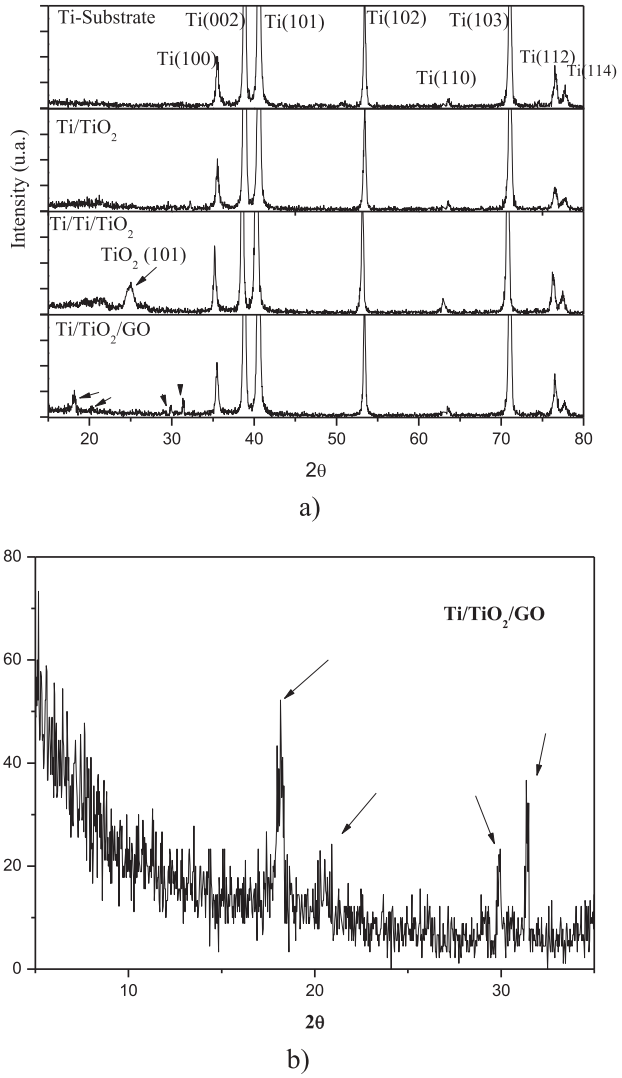

Fig. 2. a) XRD patterns of Ti, Ti/TiO_2, Ti/Ti/TiO_2 and Ti/TiO_2/GO; b) Magnified image of the Ti/TiO_2/GO XRD patterns.

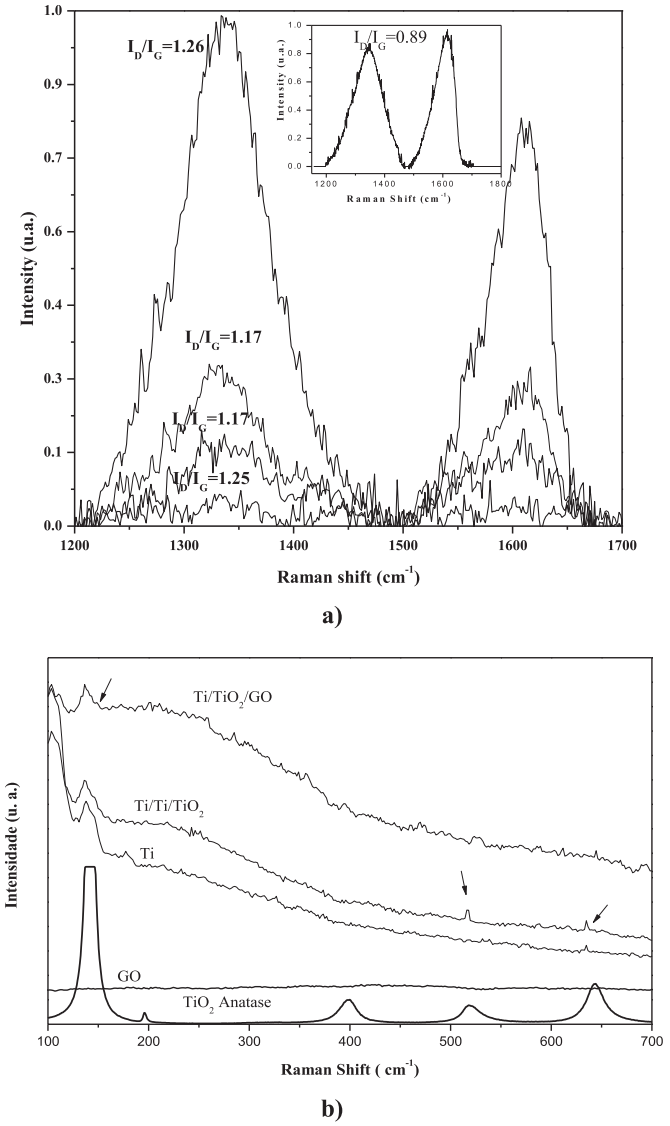

Fig. 3. Raman spectra of Ti/TiO_2/GO obtained a) in the range of 1200–1700 cm^{-1}, acquired at four different points of the surface and Inset: Raman spectra and I_D/I_G ratio value for the GO used as starting material to prepare the composite; b) in the range of 100–750 cm^{-1} in order to investigate the presence of TiO_2.

TiO_2 revealed one anatase peak at $2\theta = 25.3°$, corresponding to diffractions from the (101) plane. These results are consistent with those observed for the CVs, which showed that the addition of Ti (IV) to the electrolyte can enhance the oxide layer formation. The Ti/TiO_2/GO XRD pattern (Fig. 2(b)) shows four poorly defined peaks at $2\theta = 18.2°$, 20.6°, 29.6° and 31.2°, which could not be linked to any Ti oxides or GO typical crystal plane diffraction. This suggests that these peaks may be derived from new crystalline phases originated from the reaction of TiO_2 and GO during the anodizing process.

Raman spectroscopy is a very effective tool to investigate the detailed bonding structure of carbon-based nanostructures [26]. In this work, the surfaces of the as-prepared composite films were evaluated employing a conventional optical microscope coupled to a Raman spectrometer. Consequently, it was possible to obtain information about the film composition at different points of the substrate surface. Fig. 3(a) shows the Raman spectra of Ti/TiO_2/GO obtained at four different points of the surface. The Raman spectra obtained in the range of 1200–1700 cm^{-1} display two typical vibration modes for carbon materials. These bands were identified as D and G bands, confirming the presence of GO in Ti/TiO_2/GO. The D-band, at ~1339 cm^{-1}, is usually observed for sp^2 carbons containing impurities or other symmetry-breaking defects, while the G-band, at ~1609 cm^{-1}, is related to vibrations in sp^2 carbon materials and is attributed to well-ordered graphite [27]. Thus, a quantitative measure of functionalization density in GO can be estimated by the ratio between the areas of the D (I_D) and G bands (I_G). The I_D/I_G ratio value observed for the GO used as starting material to prepare the

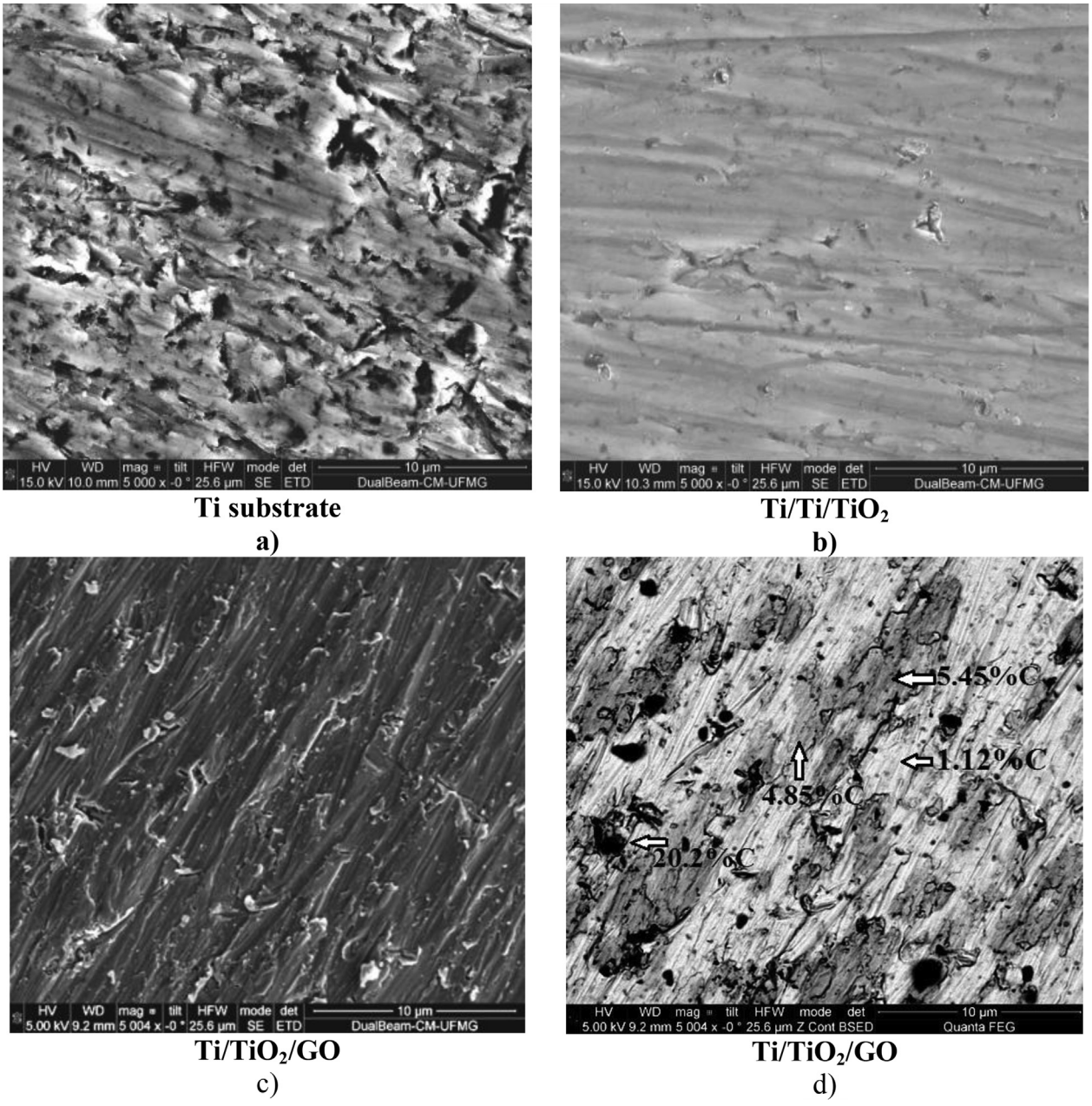

Fig. 4. SEM images of (a) Ti substrate, b) $Ti/Ti/TiO_2$, c) Ti/TiO_2/GO and d) backscattered electron image for Ti/TiO_2/GO with the carbon atomic percentage measured by EDS.

film composites is shown in the inset of Fig. 3. Thus, comparing this value with the I_D/I_G ratio values shown in Fig. 3, it can be deduced that the successive electrodeposition voltammetric cycles induced a slight decrease in the size of in-plane sp^2 domains and the expansion of the disorder in the prepared TiO_2/GO film.

The noise level discrepancy among the Raman spectra shown in Fig. 3(a) suggests that the film concentration on the substrate surface is not uniform. Thus, the composite film distribution on the Ti substrate was investigated by SEM; the results are shown in Fig. 4. The SEM image for the Ti-plate shows a surface characterized by many grooves and scratches, typical of abrasive wear. However, after film formation, the surface became smooth, as shown in Fig. 4(a–c) for Ti/Ti/TiO_2 and Ti/TiO_2/GO. Fig. 4(d) displays the backscattered electron image for Ti/TiO_2/GO. The color contrast observed in the backscattered electron image is generated by the different phase compositions relative to their average atomic number. Such differences in color distribution indicate a non-uniform film concentration on the surface, which is in agreement with the results obtained by Raman spectroscopy. The dark areas indicate the presence of lower atomic weight atoms such as C and O. Fig. 4 shows that the dark areas are located mainly in the Ti surface cracks. The GO distribution on this surface was investigated by measuring the carbon concentration by Energy-dispersive X-ray spectrometry (EDS). The measurements were collected from areas covering from light to dark regions of the surface. The EDS results are reported in Fig. 4(d). The highest carbon concentration values were found in the dark areas, which means that the film was deposited mainly in the cracks and scratches of Ti/TiO_2/GO.

The Raman spectrum region from 100 to 750 cm^{-1} was used to investigate the presence of TiO_2 [28,29]. The spectrum shown in Fig. 3(b) is very wide and exhibits a peak at ~140 cm^{-1}, observed for all samples and representative of anatase TiO_2, and a relatively broad background extending from 200 to 750 cm^{-1}. The broad continuous spectrum profile observed here is typical of amorphous semiconductors, demonstrating the predominantly amorphous structure of the oxide layer obtained by electrochemical deposition. However, sample Ti/Ti/TiO_2 showed two other bands with low intensity at 517 and 638 cm^{-1}, attributed to anatase TiO_2 [30]. These results are in agreement with those obtained by X-ray diffraction and confirm the presence of anatase TiO_2 in the prepared films.

The UV–Vis absorption properties of the as-prepared composite films on Ti substrates were measured by DRUV technique. The results are shown in Fig. 5(a). The films exhibited TiO_2 absorption characteristics with an absorption peak around 340 nm. After GO was introduced (Ti/TiO_2/GO), this peak shifted to 360 nm and the light absorbance range broadened to higher wavelength regions. Thus, the Ti/TiO_2/GO bandgap energy was reduced in relation to Ti/Ti/TiO_2 and a more efficient utilization of the solar spectrum was achieved. A similar trend has been described for other systems where GO was incorporated into TiO_2 [15–17].

Photoluminescence (PL) emission spectroscopy was used to study the transfer behavior of photo-induced electrons and holes in the composite films. In general, a decrease in the PL intensity results from a lower photo-induced electron–hole pair recombination rate and leads to photocatalytic activity increases. The measured PL-emission spectra of the films in the range of 400–850 nm are presented in Fig. 5(b). The spectra of all samples are centered around 468 nm and the intensity reduced from Ti/Ti/TiO_2 to Ti/TiO_2/GO, indicating an increase in the photocatalytic activity. The lower PL emission intensity of Ti/TiO_2/GO may be attributed to the GO action as an electron shuttle for TiO_2, preventing electron–hole recombination with a resulting higher photocatalytic activity [31].

Fig. 6(a,b) shows the photocatalytic activity results of the composite films in the degradation of Reactive Yellow 145. The

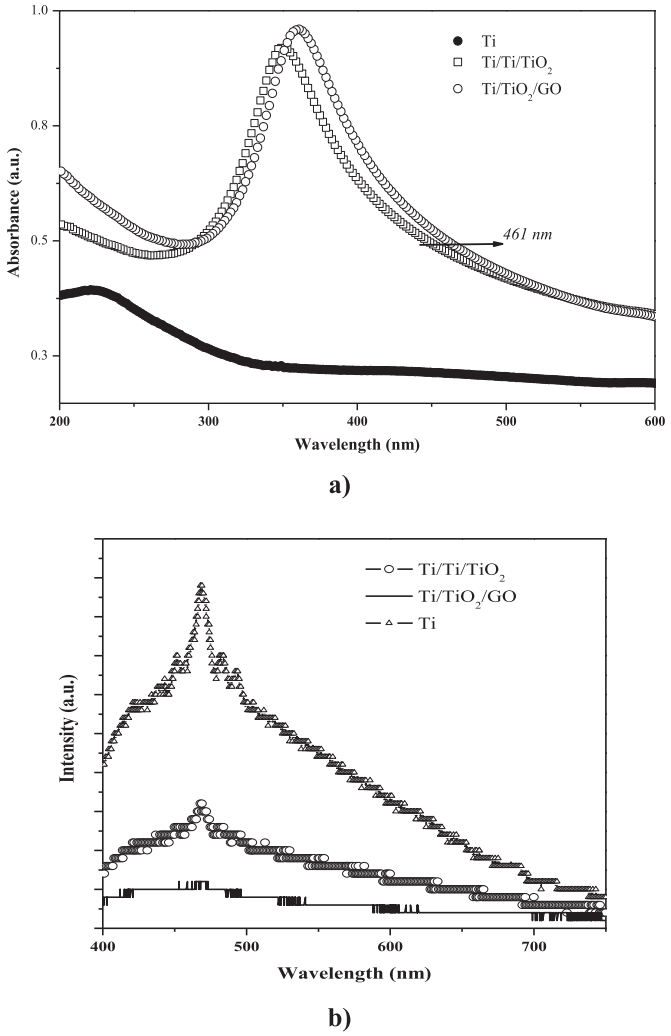

Fig. 5. a) UV–Vis absorption spectra and b) PL emission spectroscopy for the Ti substrate, Ti/Ti/TiO_2 and Ti/TiO_2/GO.

photocatalytic test was performed with a Reactive Yellow 145 synthetic solution and textile dyeing baths containing such a dye. In the case of the actual dyeing baths, other products are present besides the pigment, such as equalizing and fixing additives, acids or bases for pH control, salts and surfactants [32].

Fig. 6(a) shows that the dye concentration did not change in the first 10 min in the absence of light. The same result can be observed in Fig. 6(b) after 30 min in the dark. Similarly, no degradation occurred in the presence of the photocatalyst Ti/TiO_2/GO in the dark. On the other hand, both dye samples showed a small percentage of degradation when they were exposed to light, even in the absence of the photocatalyst.

The results depicted in Fig. 6(a,b) demonstrate that the TiO_2-based photocatalyst improved dye degradation in both samples. However, the as-prepared Ti/TiO_2/GO exhibited a higher photocatalytic activity, e.g., the rate of color removal in the first 5 min of the Reactive Yellow 145 synthetic solution in the presence of Ti/TiO_2/GO was 0.080 min^{-1}, while with Ti/Ti/TiO_2 it was only 0.045 min^{-1}. Similarly, for the textile dyeing baths, the rate of color removal employing Ti/TiO_2/GO as a catalyst was almost twice as high as with Ti/Ti/TiO_2. Thus, the addition of GO to the film improved light utilization in the degradation process by promoting

the separation of the electron–hole pairs and extending the electron life.

The stability and recyclability of photocatalysts Ti/TiO_2/GO and Ti/Ti/TiO_2 were evaluated over 15 cycles and the results are shown in Fig. 6(c–d). The exposure time was kept at 30 min. As already mentioned, the photocatalyst efficiency was lower in the absence of GO, but the behaviors of both films in the course of the different cycles were similar. Also, their photocatalytic activity reduced after the first cycle and remained on level in the subsequent cycles. However, Ti/TiO_2/GO was more efficient (≈70%) even after the last cycles. This result demonstrates that the Ti/TiO_2/GO film is reasonably stable and can be employed several times.

The reduction in the photocatalytic activity observed for Ti/TiO_2/GO may have been due to GO leaching. The Raman spectra obtained at different points on the film surface region in the range from 100 to 750 cm^{-1} were used to investigate the presence of GO in the support before and after various numbers of use cycles; the results are shown in Fig. 7. After the 12th cycle (Fig. 7(b)), the Raman spectra showed that the definition of the D and G bands was significantly reduced, suggesting that the GO concentration decreased after each application. However, it is interesting to note that GO was still present even after the 12th cycle, indicating a good adhesion between the film and the Ti substrate.

4. Conclusions

In summary, Ti/TiO_2/GO and Ti/Ti/TiO_2 composite films were prepared by electrodeposition onto a Ti substrate. Raman, SEM and EDS measurements showed that the film distribution on the substrate surface was not uniform, being deposited mainly into cracks and scratches. The as-prepared composite films exhibited characteristic TiO_2 absorption; however, Ti/TiO_2/GO exhibited a red shift on the band-edge at about 461 nm. The Ti/TiO_2/GO film showed the lowest PL emission intensity, which was associated with GO acting as an electron shuttle for TiO_2 with a resulting delay in the electron–hole recombination. The photocatalytic properties of the as-prepared films were investigated for the discoloration of Reactive Yellow 145 dye. The photocatalytic activity of Ti/TiO_2/GO was almost twice as high as that of Ti/Ti/TiO_2. In addition, Ti/TiO_2/GO presented a higher stability and recyclability, retaining its catalytic efficiency (≈70%) even after 15 cycles.

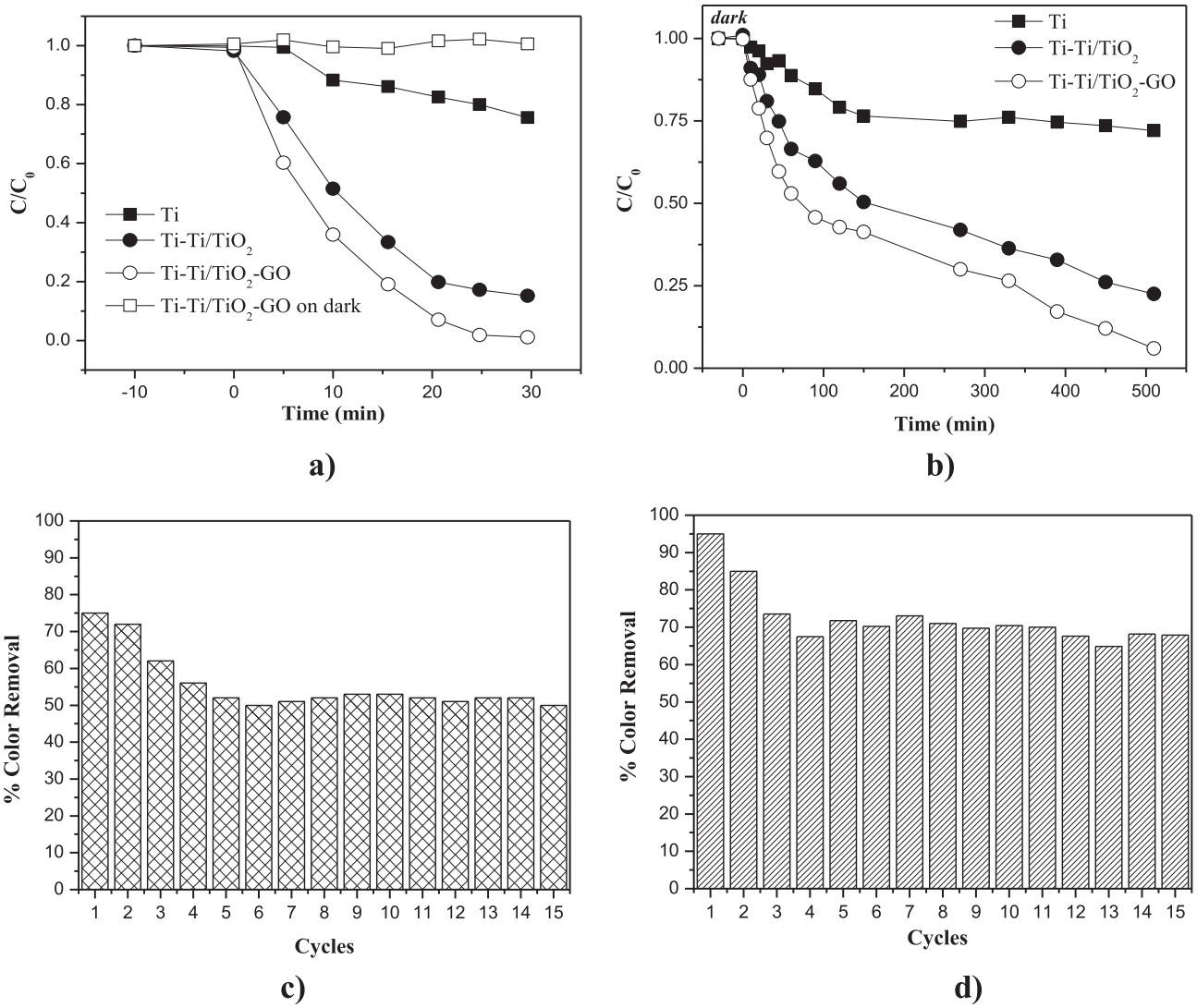

Fig. 6. Photocatalytic activity for the photodegradation of a) Reactive Yellow 145 synthetic solution, and b) the textile dyeing baths containing Reactive Yellow 145; Percentage of dye degradation in the Reactive Yellow 145 synthetic solution obtained over 15 film reuse cycles: c) Ti/Ti/TiO_2 and d) Ti/TiO_2/GO.

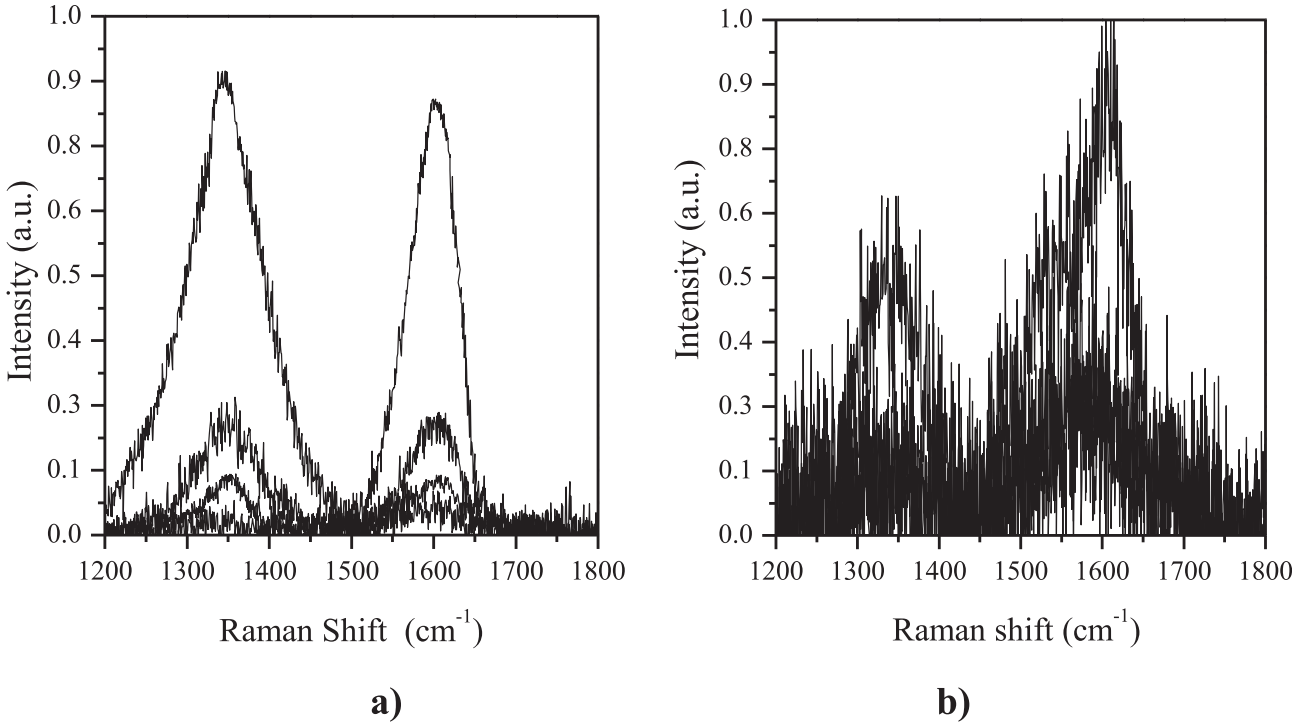

Fig. 7. Raman spectra of Ti/TiO_2/GO obtained at four different points on the film surface in the range of 100–750 cm^{-1} (a) before and (b) after 15 use cycles.

Acknowledgment

This research was supported by the Brazilian Agencies FAPEMIG (CEX - APQ-01870-14), FINEP (convenio 01.09.0399.00), CNPq, CAPES (FQMat doctoral scholarship), Brazilian Institute of Nanotechnology (INCT) and Microscopy Center of UFMG. This work was co-financed by FCT/MEC, FEDER under Programe PT2020 (Project UID/EQU/50020/2013).

References

[1] T.T. Guaraldo, T.B. Zanoni, S.I.C. Torresi, et al., On the application of nanostructured electrodes prepared by Ti/TiO_2/WO_3 "template": a case study of removing toxicity of indigo using visible irradiation, Chemosphere 91 (2013) 586–593.
[2] T. Ochiaia, A. Fujishima, Photoelectrochemical properties of TiO_2 photocatalyst and its applications for environmental purification, J. Photochem. Photobiol. C 13 (2012) 247–262.
[3] S.Y. Lee, S.J. Park, TiO_2 photocatalyst for water treatment applications, J. Ind. Eng. Chem. 19 (2013) 1761–1769.
[4] L. Zhang, H.H. Mohamed, R. Dillert, D. Bahnemann, Kinetics and mechanisms of charge transfer processes in photocatalytic systems: a review, J. Photochem. Photobiol. C 13 (2012) 263–276.
[5] M.N. Chong, B. Jin, C.W.K. Chow, C. Saint, Recent developments in photocatalytic water treatment technology: a review, Water Res. 44 (2010) 2997–3027.
[6] W. Wang, P. Serp, P. Kalck, J.L. Faria, Visible light photodegradation of phenol on MWNT-TiO2 composite catalysts prepared by a modified sol-gel method, J. Mol. Catal. A Chem. 235 (2005) 194–199.
[7] W. Wang, P. Serp, P. Kalck, J.L. Faria, Photocatalytic degradation of phenol on MWNT and titania composite catalysts prepared by a modified sol-gel method, Appl. Catal. B Environ. 56 (2005) 305–312.
[8] L.M. Pastrana-Martínez, S. Morales-Torres, S.K. Papageorgiou, et al., Photocatalytic behaviour of nanocarbon-TiO2 composites and immobilization into hollow fibres, Appl. Catal. B Environ. 142–143 (2013) 101–111.
[9] L.M. Pastrana-Martínez, S. Morales-Torres, V. Likodimos, et al., Advanced nanostructured photocatalysts based on reduced graphene oxide-TiO2 composites for degradation of diphenhydramine pharmaceutical and methyl orange dye, Appl. Catal. B Environ. 123–124 (2012) 241–256.
[10] Q. Xiang, J. Yu, M. Jaroniec, Graphene-based semiconductor photocatalysts, Chem. Soc. Rev. 41 (2012) 782–796.
[11] L.M. Pastrana-Martínez, S. Morales-Torres, V. Likodimos, et al., Role of oxygen functionalities on the synthesis of photocatalytically active graphene-TiO2 composites, Appl. Catal. B Environ. 158–159 (2014) 329–340.
[12] L.M. Pastrana-Martínez, S. Morales-Torres, S. Carabineiro, et al., Nanodiamond-TiO2 composites for heterogeneous photocatalysis, ChemPlusChem 78 (2013) 801–807.
[13] L. Hu, S. Dong, Q. Li, et al., Facile synthesis of BiOF/Bi2O3/reduced graphene oxide photocatalyst with highly efficient and stable natural sunlight photocatalytic performance, J. Alloys Compd. 633 (2015) 256–264.
[14] H. Xie, X. Ye, K. Duan, et al., CuAu–ZnO–graphene nanocomposite: a novel graphene-based bimetallic alloy-semiconductor catalyst with its enhanced photocatalytic degradation performance, J. Alloys Compd. 636 (2015) 40–47.
[15] C. Liu, Y. Teng, R. Liu, et al., Fabrication of graphene films on TiO_2 nanotube arrays for photocatalytic application, Carbon 49 (2011) 5312–5320.
[16] P. Solís-Fernández, R. Rozada, J.I. Paredes, et al., Chemical and microscopic analysis of graphene prepared by different reduction degrees of graphene oxide, J. Alloys Compd. 536 (2012) S532–S537.
[17] W. Jo, H. Kang, Titanium dioxide-graphene oxide composites with different ratios supported by pirex tube for photocatalysis of toxic aromatic vapors, Powder Technol. 250 (2013) 115–121.
[18] W.S. Hummers, R.E. Offeman, Preparation of graphitic oxide, J. Am. Chem. Soc. 80 (1958), 1339–1339.
[19] D.C. Marcano, D.V. Kosynkin, J.M. Berlin, et al., Improved synthesis of graphene oxide, ACS Nano 4 (2010) 4806–4814.
[20] V. Antonucci, N. Giordano, J. Bart, Structure and photoelectrochemical efficiency of oxidized titanium electrodes, Int. J. Hydrogen Energy 7 (1982) 769–774.
[21] M.P. Neupane, I.S. Park, S.J. Lee, et al., Study of anodic oxide films of titanium fabricated by voltammetric technique in phosphate buffer media, Int. J. Electrochem. Sci. 4 (2009) 197–207.
[22] I.S. Park, M.H. Lee, T.S. Bae, K.W Seol, Effects of anodic oxidation parameters on a modified titanium surface, J. Biomed. Mater. Res. Part B 84B (2008) 422–429.
[23] K. Thamaphat, P. Limsuwan, B. Ngotawornchai, Phase characterization of TiO_2 powder by XRD and TEM, Kasetsart J. Nat. Sci. 42 (2008) 357–361.
[24] D.R. Coronado, G.R. Gattorno, M.E.E. Pesqueira, et al., Phase-pure TiO_2 nanoparticles: anatase, brookite and rutile, Nanotechnology 19 (2008) 145605–1456015.
[25] D. Rafaja, V. Klemm, G. Schreiber, et al., Interference phenomena observed by X-ray diffraction in nanocrystalline thin films, J. Appl. Crystallogr. 37 (2004) 613–620.
[26] P.K. Chu, L. Li, Characterization of amorphous and nanocrystalline carbon films, Mater. Chem. Phys. 96 (2006) 253–277.
[27] A.C. Ferrari, Raman spectroscopy of graphene and graphite: disorder, electron–phonon coupling, doping and nonadiabatic effects, Solid State Commun. 143 (2007) 47–57.
[28] H.C. Choi, Y.M. Jung, S.B. Kim, Size effects in the Raman spectra of TiO_2 nanoparticles, Vib. Spectrosc. 37 (2005) 33–38.

[29] H.C. Choi, Y.M. Jung, S.B. Kim, Characterization of Raman spectra of size-selected TiO_2 nanoparticles by two-dimensional correlation spectroscopy, Bull. Korean Chem. Soc. 25 (2004) 426–428.
[30] P. Wang, Y. Zhai, D. Wang, et al., Synthesis of reduced graphene oxide-anatase TiO_2 nanocomposite and its improved photo-induced charge transfer properties, Nanoscale 3 (2011) 1640–1645.
[31] J. Liqiang, Q. Yichun, W. Baiqi, et al., Review of photoluminescence performance of nano-sized semiconductor materials and its relationships with photocatalytic activity, Sol. Energy Mater. Sol. Cells 90 (2006) 1773–1787.
[32] Ş. Gül, Ö. Özcan-Yıldırım, Degradation of reactive red 194 and reactive yellow 145 azo dyes by O_3 and H_2O_2/UV-C processes, Chem. Eng. J. 155 (2009) 684–690.